
Theoretical Studies on the Hydrolysis of Phosphate Diesters in the Gas Phase, Solution, and RNase A

XABIER LOPEZ,^{1,2,3} DARRIN M. YORK,⁴ ANNICK DEJAEGERE,⁵
MARTIN KARPLUS^{2,6}

¹*Kimika Fakultatea, Euskal Herriko Unibertsitatea, P.K. 1072, 20080 San Sebastian, Spain*

²*Laboratoire de Chimie Biophysique, Institut le Bel, Université Louis Pasteur, 67000 Strasbourg, France*

³*Oxford Centre for Molecular Sciences, New Chemistry Lab., South Parks Road, Oxford OX1 3QZ, United Kingdom*

⁴*Department of Chemistry, University of Minnesota, 207 Pleasant St. SE, Minneapolis, Minnesota 55455-0431*

⁵*Laboratoire de Biologie et Génomique Structurales, Ecole Supérieure de Biotechnologie de Strasbourg, 67400 Illkirch, France*

⁶*Department of Chemistry and Chemical Biology, Harvard University, Cambridge, Massachusetts 02138*

Received 4 October 2000; revised 24 April 2001; accepted 2 May 2001

ABSTRACT: Density functional theory, polarizable continuum models and semiempirical hybrid quantum mechanical/molecular mechanical (QM/MM) calculations were applied to the hydrolysis of phosphate diesters in the gas phase, in solution, and in the enzyme RNase A. Neutralization of the negative charge of the pentacovalent phosphorane intermediates provides a substantial stabilization of the transition-state structures in the gas phase. Inclusion of solvent effects on the phosphate/phosphorane species was critical to reproducing the trends in reactivity observed experimentally. Finally, the catalytic mechanism for the hydrolysis of uridine 2',3'-cyclic phosphate by RNase A was studied by QM/MM calculations. Our results suggest that the rate-limiting transition state of the reaction corresponds to the approach of a water molecule to the phosphate and its activation by His119. Thus, His119 acts as a generalized base for the reaction. The water attack leads to a pentacovalent phosphorane transition state of formal charge -2 ; this excess of negative charge in the transition state is stabilized by a number of positively charged residues including His12 and Lys41. In the second stage of the reaction, the phosphorane is converted into products. This part of the reaction proceeds without a detectable barrier, and it is facilitated by a proton transfer from Lys41 to the departing O_2^- . © 2002 John Wiley & Sons, Inc. *Int J Quantum Chem* 86: 10–26, 2002

Correspondence to: X. Lopez; e-mail: poplopex@sq.ehu.es.

Contract grant sponsors: European Commission; National Institutes of Health; Minnesota Supercomputing Institute; Donors of The Petroleum Research Fund.

Key words: QM/MM; hydrolysis; phosphate; RNase A

Introduction

Phosphate diesters play a fundamental role in biology since they are the chemical group that link nucleotides in deoxyribonucleic acid (DNA) and ribonucleic acid (RNA) [1]. The chemical properties and reactivity of phosphates determine how they are formed and cleaved, and therefore, phosphate diesters have been the subject of numerous theoretical and experimental studies [2–12]. A particular case that has received much attention is the cleavage of RNA [13–17], through the hydrolysis of its phosphate diester linkage. The cleavage occurs in two related steps: transphosphorylation and hydrolysis (Fig. 1). In the first step, the 2' oxygen acts as a nucleophile and attacks the phosphorus. This leads to the cleavage of the 5'CH₂O–P bond to a nucleotide and results in a 2',3'-cyclic phosphate. In the second step, the attacking nucleophile is OH[−] at high pH, and as a result of the attack, the ring is broken and the OH group in the 2' position is regenerated. We have carried out extensive theoretical studies in order to understand the hydrolysis step of the reaction in RNase A. A first step is to analyze the gas-phase chemistry displayed by small model compounds such as ethylene phosphate (EP[−]). However, the reactions *in vivo* are catalyzed by enzymes in solution. Therefore, a complete understanding of the biological reactivity of these molecules requires detailed study of the role of the solvent and enzyme environment.

In this study, we describe applications of theoretical methods to study the hydrolysis of several phosphate diester molecules that serve as models for the cleavage of RNA. The following section

briefly outlines the methods that were applied in each of the calculations, and the third section presents and discusses results, including the results of gas-phase density-functional calculations of hydroxide and water attack on ethylene phosphate (EP[−]) and on the water attack on protonated ethylene phosphate (EPH). Then the gas phase results are compared with calculations of the alkaline hydrolysis of phosphate and sulfate compounds in solution [5, 7, 18] using a continuum solvent model [19–21]. Finally, the effect of the enzyme environment on the cleavage of uridine 2',3'-cyclic phosphate catalyzed by bovine ribonuclease A (RNase A) using a combined quantum mechanical/molecular mechanical (QM/MM) approach [22–24] is examined. This series of calculations provides a comprehensive view of the main factors affecting the energetics of these reactions in the gas phase, in solution, and in the enzyme.

Methods

GAS-PHASE CALCULATIONS

All the structures in the gas phase were optimized at the B3LYP/6-31G+(d) level of theory [25–28]. Frequency calculations were performed to verify that stationary points were transition states (one imaginary frequency) or minima (no imaginary frequencies) on the potential energy surface (PES). After geometry optimization, the energetics were refined with a larger basis set 6-311++G(3df,2p). This is a basis set similar to the one used in the G2 method [29], which yield atomization energies, ionization energies, and relative energies within

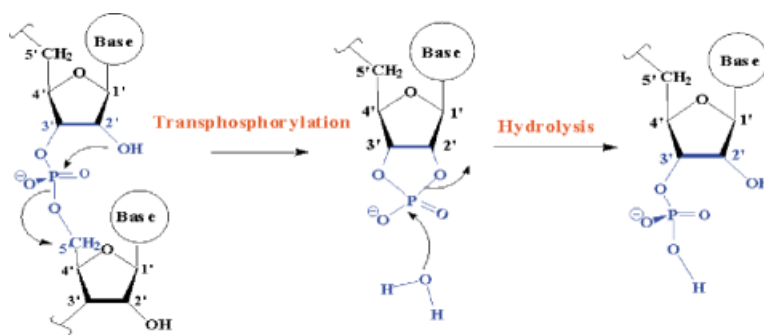


FIGURE 1. Transphosphorylation and hydrolysis steps in the cleavage of RNA.

1 kcal/mol of experimental values. All the calculations were done with the GAUSSIAN98 suite of programs [30].

POLARIZABLE CONTINUUM MODEL

Solvent effects were treated using the polarizable continuum model of Tomasi [19–21]. In this model, the solute molecule is embedded in a cavity of unit dielectric that is surrounded by solvent modeled by a dielectric continuum. The solute and solvent are coupled by a reaction potential of the dielectric medium in response to the solute charge distribution. The polarization of the solvent is represented by a charge density σ introduced on the surface S of the cavity surrounding the solute, and the corresponding reaction field potential takes the form

$$\phi(\mathbf{r}) = \int_S d^2s \frac{\sigma(\mathbf{s})}{|\mathbf{r} - \mathbf{s}|}. \quad (1)$$

Solvent calculations were performed at the B3LYP/6-31+G(d) level of theory using GAUSSIAN94 [31].

QM/MM CALCULATIONS

In QM/MM calculations [22–24] the Hamiltonian is divided in three components:

$$\hat{H} = \hat{H}_{\text{QM}} + \hat{H}_{\text{QM/MM}} + \hat{H}_{\text{MM}}, \quad (2)$$

where \hat{H}_{QM} is the quantum mechanical Hamiltonian operator, \hat{H}_{MM} is the classical molecular mechanics Hamiltonian, and $\hat{H}_{\text{QM/MM}}$ is the coupling term [32]. In this work, we use a new AM1/d semiempirical model with specific parameterization to reproduce

energetics of nucleophilic attack to phosphate diesters. The model Hamiltonian and new parameterization will be described in detail elsewhere [33], and it is based on a modification of the MNDO97 semiempirical package [34]. The molecular mechanical (MM) part was modeled with the all-atom force field [35] within the CHARMM [36] molecular modeling suite.

The QM/MM Hamiltonian consists of an electrostatic interaction between the partial atomic charges of the MM part and the electrons and nuclei of the quantum part plus a van der Waals term:

$$\hat{H}_{\text{QM/MM}} = - \sum_{i,M} \frac{q_M}{r_{i,M}} + \sum_{\alpha,M} \frac{Z_\alpha q_M}{R_{\alpha,M}} + \sum_{\alpha,M} \left(\frac{A_{\alpha,M}}{R_{\alpha,M}^{12}} - \frac{B_{\alpha,M}}{R_{\alpha,M}^6} \right). \quad (3)$$

The PES was investigated by a series of minimizations using the steepest descents (SD) and adaptive basis Newton–Raphson (ABNR) algorithms in CHARMM, with selected distances restrained with a harmonic potential (force constant of 2000 kcal mol⁻¹ Å⁻²). We henceforth refer to these minimizations as *resd* (restrained distance) minimizations in the text. To optimize structures that are minima on the PES (i.e., the reactant and product of the reaction), the harmonic restraints were removed, and we performed ABNR minimizations until the norm of the gradient was below 0.001 kcal/mol Å. Transition-state search was performed using the conjugate peak refinement (CPR) algorithm [37] in CHARMM.

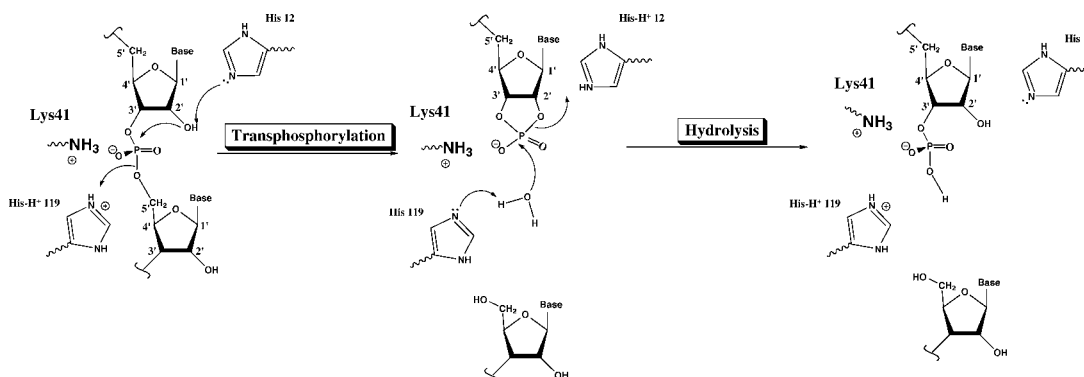


FIGURE 2. Cleavage of RNA catalyzed by RNase A. Classically proposed mechanism [40] in which His12 and His119 act as acid-base catalysts of the reaction and Lys41 is electrostatically stabilizing the negative charge of the phosphate/phosphorane along the reaction coordinate.

Results and Discussion

GAS-PHASE RESULTS

We have characterized the transition states, phosphorane intermediates and products for the hydroxide and water attack on ethylene phosphate, and water attack on protonated ethylene phosphate. The total charge of each reaction is different. The hydroxide attack on ethylene phosphate is a dianionic PES, water attack on EP^- is a monoanionic, and the water attack on EPH is neutral. In all cases, the rate-limiting transition state corresponds to the attack of the nucleophile on the phosphate that leads a pentacovalent phosphorane. We refer to these transition states as TS1^i with $i = -2, -1, 0$ indicating the total charge of the molecule. Stable pentaco-

valent intermediates (INT^i) could only be found for the monoanionic and neutral PES ($i = 0, -1$). All TS1 and INT structures are shown in Figure 3. We also characterized the transition states that correspond to the cleavage of P–O axial ester bond (TS2^i). All of these transition states were found to be lower in energy than the TS1 structures, so that they are not predicted to correspond to the rate-limiting step of the reaction. The relative energies of all the stationary points can be found in Table I.

Energies

The gas-phase hydroxide attack on EP^- requires a high energy for activation ($\Delta E^{\text{TS1}^{-2}} = 85.0$ kcal/mol). This reaction and its acyclic counterpart (OH^- attack on DMP^-) have been well described in previous theoretical work [4–7, 12], and

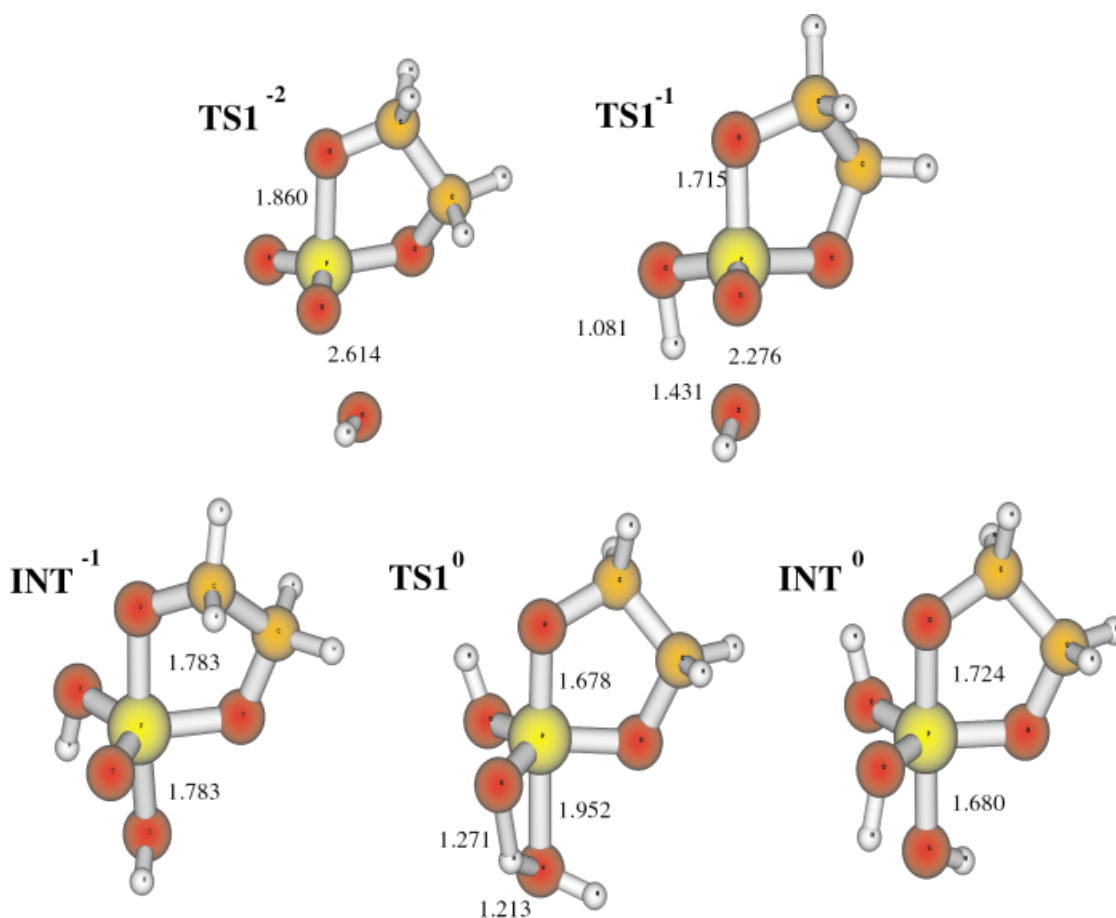


FIGURE 3. Gas-phase structures for the rate-limiting transition state (TS1) of hydroxide attack on ethylene phosphate (TS1^{-2}), water attack on ethylene phosphate (TS1^{-1}), and water attack on protonated ethylene phosphate (TS1^0). The phosphorane intermediates (INT) of the reaction are also shown. Geometries determined at the B3LYP/6-31+G* level of theory.

TABLE I
Relative energies, in kcal/mol, with respect to the reactants for the gas-phase hydrolysis of ethylene phosphate and protonated ethylene phosphate.^a

	EP ⁻ + OH ⁻	EP ⁻ + OH ₂	EPH + OH ₂
TS1	87.2	23.3	26.9
INT		14.3	1.3
TS2		14.4	20.0
PROD	35.1	-9.7	-9.5

^a TS1 is the transition state for the attack of the nucleophile and formation of the phosphorane intermediate (INT). TS2 is the transition state that leads from the phosphorane intermediates to the products (PROD).

our results do not differ significantly from these conclusions. The origin of the high barrier is the coulombic repulsion for the approach of two anions (OH⁻ and EP⁻) in the gas phase. Any attempt to trap a pentacovalent phosphorane intermediate failed and led to the collapse of the structure into the more extended phosphate product. Nevertheless, we can give an estimate for the relative energy of the dianionic phosphorane intermediate based on previous studies where partial optimizations were done with the P-O axial bonds frozen. It was found that the dianionic pentacovalent phosphorane structure is 75–80 kcal/mol higher in energy than the reactants.

Next, we analyze the water attack on ethylene phosphate. This is a more complex reaction in that the nucleophilic attack is concerted with a proton transfer from the water to one of the phosphoryl oxygens (Fig. 3). The transition state is lowered to 25.0 kcal/mol relative to the reactants, although the barrier in the gas phase should be measured with respect to an ion-molecule complex (not shown) formed at initial stages of the reaction. The ion-molecule complex is 15 kcal/mol lower in energy than the reactants, so that the gas-phase energy barrier between the ion-molecule complex and TS1 is 40 kcal/mol. The energy of the monoanionic phosphorane intermediate INT⁻¹ is 14.3 kcal/mol, remarkably more stable than the estimate for the dianionic phosphorane intermediate (around 75–80 kcal/mol). Depending on the orientation of the proton in the phosphoryl oxygen, one can find different intermediates, but their energy is within 1 kcal/mol of the intermediate shown in Figure 3. The transition state for the cleavage of the phosphorane intermediate (TS2⁻¹) is 14.5 kcal/mol higher in

energy than the reactants, and the reaction energy is -9.7 kcal/mol.

Finally, we examine water attack on EPH. The rate-limiting transition state of the reaction corresponds again to the water attack on the phosphate with simultaneous proton transfer from the water to one of the phosphoryl oxygens concerted with nucleophilic attack. The energy barrier for the reaction is 26.9 kcal/mol. The energy of the neutral phosphorane intermediate INT⁰ is 1.3 kcal/mol relative to the reactants, which makes it the most stable phosphorane intermediate of the series studied here. As a result, the barrier for the cleavage to products increases to 18.7 kcal/mol: The second transition state (TS2⁰) is 20 kcal/mol higher in energy than the reactant. Finally, the reaction energy of the neutral reaction PROD⁰ (-9.5 kcal/mol) is similar to the monoanionic value PROD⁻¹ (-9.7 kcal/mol).

Transition-State Structures

An interesting trend in these reactions is how the geometry of the transition state changes with the amount of negative charge of the system (Fig. 3) with the mechanism being increasingly associative as the charge diminishes. For TS1⁻², the P-OH distance is 2.614 Å and the P-O_{ax} distance is 1.860 Å. These distances decrease significantly in TS1⁻¹, 2.276 Å for P-OH and 1.715 Å for P-O_{ax}. Finally, for the neutral transition state, TS1⁰, we get the most associative structure with a P-OH distance of 1.952 Å and a P-O_{ax} distance of 1.678 Å. There is an important difference in the degree of proton transfer carried out at the transition state. In TS1⁻¹, the proton transfer from water to one of the phosphoryl oxygens is almost complete. The H-OH distance is 1.431 Å and the H-O_{phos.} is only 1.081 Å. However, in the case of TS1⁰, the proton is almost equidistant from the water and phosphoryl oxygens (H-OH is 1.213 Å and H-O_{phos.} is 1.271 Å).

Summary

As the nucleophilic attack takes place, a pentacovalent phosphorane with a bipyramid trigonal structure is formed. There is a very clear correlation between the total negative charge of the phosphorane and its gas-phase stability with respect to the reactants: The lower the negative charge in the phosphorane the greater the stability. The coulombic repulsion of the anions is thus a key factor in the destabilization of the pentacovalent phosphorane intermediates. The neutralization of the net

charge is of fundamental importance to stabilizing the reaction in the gas phase. Complete neutralization leads to the lowest activation barrier (TS1) but increases the relative activation barriers for cleavage of the phosphorane (TS2). Charge neutralization also increases association. Thus, the P–OH distance in the transition state shows a remarkable degree of contraction as the negative charge of the system decreases: the P–OH distance for TS1 is 2.614 Å for TS1⁻², 2.276 Å for TS1⁻¹, and 1.952 Å for TS1⁰.

EFFECT OF SOLVENT

Phosphates are negatively charged species at physiological pH. Based on the gas-phase results, the stabilization of the excess negative charge in the phosphorane intermediates is a key factor in lowering the energetic barrier of the reaction. Water constitutes a high dielectric medium that plays a large role in reactions that take place *in vivo*. The stabilization of charged species in solution can have a tremendous effect on reactivity. In this section, we discuss the origin of the rate acceleration of cyclic versus acyclic phosphates and sulfates in solution.

Hydrolysis of cyclic phosphates/sulfates is 10⁷ times faster than hydrolysis of their acyclic analogs in solution at ambient conditions. This implies a differential barrier ($\Delta\Delta G^\ddagger$) of around -10 kcal/mol for the transition states of the hydrolysis of cyclic versus acyclic compounds. The classical explanation of this behavior is that ring strain destabilizes the cyclic reactants, and therefore, the lower the activation barrier for the hydrolysis of the cyclic compounds [38, 39].

Table II shows the calculated barriers in the gas phase and in solution for the hydrolysis of EP⁻, DMP⁻, ES, and DMS. Figure 4 illustrates the corresponding transition-state structures. We used the B3LYP functional [25–28] for all density functional calculations and the PCM [19–21] with dielectric ϵ of 80 to model the effect of the solvent on the reaction (see Ref. [18] for further details). The important result from Table II is that gas-phase calculations for the alkaline hydrolysis of phosphates, and sulfates do not reproduce the experimentally observed $\Delta\Delta G^\ddagger$ for the difference in activation between the cyclic and acyclic compounds. The barrier for the hydrolysis of phosphates is very high and corresponds to the approach of the two negative anions, 95.65 kcal/mol for EP⁻ and 94.62 kcal/mol for DMP⁻. The relative energy of the barrier heights ($\Delta\Delta G^\ddagger = +1$ kcal/mol) is in contrast with the experimental observations of the relative rates. In the

TABLE II Relative free energies (kcal/mol) with respect to the reactants for the transition states of the alkaline hydrolysis of EP⁻, DMP⁻, ES, and DMS in the gas phase ($\Delta G_{\text{gas}}^\ddagger$) and in aqueous solution ($\Delta G_{\text{aq}}^\ddagger$).^a

Reactant	$\Delta G_{\text{gas}}^\ddagger$	$\Delta\Delta G_{\text{gas}}^\ddagger$	$\Delta G_{\text{aq}}^\ddagger$	$\Delta\Delta G_{\text{aq}}^\ddagger$
EP ⁻ + OH ⁻	95.7	+1.1	26.9	-8.1
DMP ⁻ + OH ⁻	94.6		37.7	
ES + OH ⁻	4.8	10.3	17.2	-5.8
DMS + OH ⁻	-5.5		23.0	

^a Data taken from Ref. [18]. The $\Delta\Delta G^\ddagger$ values correspond to the differences in the barrier between the cyclic and acyclic cases, which should be compared with the experimental value [38] (approximately -10 kcal/mol value).

case of sulfates the barriers are lower than for the phosphates, 4.8 kcal/mol for the hydrolysis of ES and -5.5 kcal/mol for that of the DMS, as a result of the difference in total charge, since for sulfates we have the attack of OH⁻ on a neutral molecule. In terms of differential barrier between the hydrolysis of cyclic and acyclic molecules, the gas-phase barrier for the cyclic compound is higher than for the acyclic one (namely, $\Delta\Delta G^\ddagger$ is +10.3 kcal/mol), which clearly does not explain the experimental data [38].

When solvent corrections are included, the barrier heights change dramatically. In the case of phosphates, the barrier heights are lowered by the solvent. The calculated activation free energies are 37.7 and 29.6 kcal/mol for DMP⁻ and EP⁻. The origin of this stabilization is that the solvation free energy varies with the square of the charge (e.g., Born model). The reactants each have a total charge of -1, and the transition state has a charge of -2, so that larger solvation free energies can be expected for the transition state than for the separate reactants. In the case of sulfates the effect is opposite. The sulfate reactant is neutral, so that there is no change in total charge as the hydroxide attack takes place. In this case, the barrier heights increases when we add the solvent corrections, since as the attack proceeds there is delocalization of the concentrated negative charge of hydroxide on the whole molecular system. This leads to a lowering of the charge density in the transition state and therefore a less favorable solvation. The free energy barriers for the hydrolysis of ES and DMS are 17.2 kcal/mol and 23.0 kcal/mol, respectively.

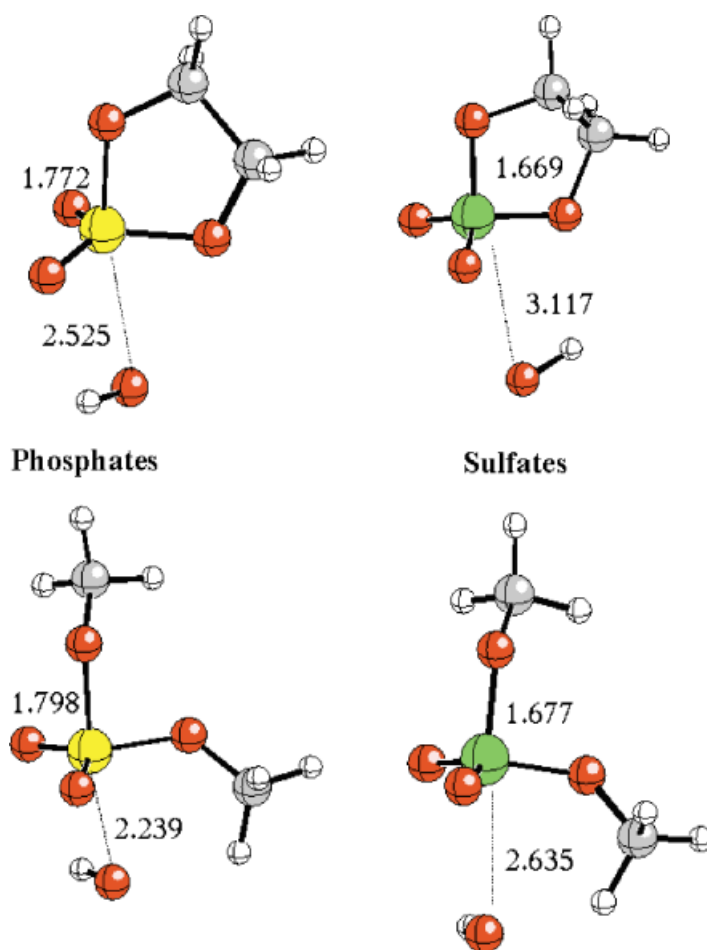


FIGURE 4. Transition states in the alkaline hydrolysis of ethylene phosphate (top left-hand side), dimethyl phosphate (bottom left-hand side), ethylene sulfate (top right-hand side), and dimethyl sulfate (bottom right-hand side). Structures determined at the B3LYP(SCI-PCM)/6-31+G* level of theory (see Ref. [18] for details).

The overall effect of solvent significantly alters the activation energies of the cyclic and acyclic phosphates (26.9 and 37.7 kcal/mol, respectively) and sulfates (17.2 and 23.0 kcal/mol, respectively), and reverses the gas-phase trend of the relative activation energies. The $\Delta\Delta G^\ddagger$ values for the cyclic versus acyclic hydrolysis reactions in solution become -8.1 and -5.8 kcal/mol for the phosphate and sulfate systems, respectively. These values are in much closer agreement with the experimentally inferred value of around -10 kcal/mol, although slightly smaller [38]. The origin of the stabilization of the cyclic transition states over the acyclic ones is the smaller solvation free energies for the latter due to the partial shielding of the hydroxide by the equatorial methoxy groups in the acyclic com-

pounds (see Fig. 4). In the case of cyclic compounds, the ring geometries maintain the aliphatic groups in a conformation away from the incoming nucleophile so that the OH^- group is more exposed to the solvent.

In summary, we have seen in this section that the solvent has an essential influence on the reaction barriers for these reactions, to the point that gas-phase calculations give the wrong trend in reactivity for these compounds. The fact that phosphates are charged species, and that the localization of the negative charge changes along the reaction coordinate, underscores the importance of inclusion of solvation in these calculations.

In the following section, we examine how the phosphate hydrolysis reactions are stabilized in the

enzyme environment. Since this environment is vastly more complex, we use a hybrid QM/MM approach.

ENZYME CATALYSIS

The hydrolysis of RNA *in vivo* is catalyzed by ribonucleases [1]. To elucidate the role of the enzyme in the catalysis, we have performed QM/MM calculations on the hydrolysis of RNA catalyzed by bovine ribonuclease A (RNase A) [15]. Mutation experiments indicate that His12, His119, and Lys41 are critical residues for the catalytic activity [15]. The classical proposed mechanism [40] is one in which the two His act as general acid-base catalysts and the positively charged Lys41 stabilizes the excess of negative charge on the phosphorane (Fig. 2). For the hydrolysis step of the cleavage of RNA, the mechanism implies that His119 activates the nucleophilic water by removing one of the protons (i.e., general base catalysis) and His12 activates the P–O₂ bond in the hydrolysis step by protonation of the O₂ oxygen (i.e., general acid catalysis). However, this view has been questioned recently by kinetic experiments [41–43] of the cleavage and isomerization of dinucleotides in imidazole buffer. Using these observations, Breslow proposed [41] a mechanism in which neutralization of substrate occurs in conjunction with nucleophilic attack at the phosphorus. On the basis of *ab initio* quantum mechanical results of a model substrate in the gas phase, Lim and Tole [6, 44, 45] have also supported the idea of neutralization of the phosphate substrate in the transphosphorylation process. In addition, His119 would stabilize the substrate through interaction with one of the nonbridging phosphoryl oxygen. The role of Lys41 is also a subject of controversy. In the classical mechanism, Lys41 in its protonated form, stabilizes the substrate through electrostatic interactions with the negatively charged phosphoryl oxygens. Mutagenesis experiments by Messmor et al. [46], which introduces nonnatural amino acid residues at position 41 in RNase A suggested that Lys41 donates a single hydrogen bond to the rate-limiting transition state during catalysis. However, Wladkowski et al. [9, 10, 47] have proposed a more prominent role for Lys41, in which Lys41 could undergo a formal proton transfer. Recently the activation barriers for the monoanionic and dianionic mechanism of the transphosphorylation step of the reaction have been estimated by Glennon et al. [48] with the empirical valence bond method [49], resulting in the conclusion that there is a similar probab-

ity for both mechanisms with slightly stronger support for the dianionic mechanism. We decided to investigate the hydrolysis reaction in the enzyme with QM/MM calculations on the UV-RNase A complex (see above), using a new AM1/d Hamiltonian for phosphate hydrolysis, the details of which are forthcoming [33]. Preliminary calculations showed that a dianionic mechanism was of slightly lower energy (by 2–3 kcal/mol) than a monoanionic mechanism where one of the phosphoryl oxygens of the phosphorane intermediate was protonated by His12. For the sake of brevity, we only present the results obtained for the dianionic mechanism.

Preparation of the Structure

We departed from a 1.3 Å high-resolution X-ray structure of RNase A bound to uridine vanadate [47, 50]. Uridine vanadate forms a pentacovalent trigonal bipyramidal structure similar to the conformation adopted by the presumed phosphorane transition state/intermediate of the reaction. In our calculations we substitute the central vanadium atom by phosphorus, and henceforth refer to the system as the uridine 2,3'-cyclic phosphorane (UP) structure. Hydrogen positions were initially calculated using the HBUILD command [51] within CHARMM [36]. In order to simplify the calculations, we focused our studies on a localized region around the active site. We solvated UP-RNase A with a 16-Å sphere of water around the central phosphorus atom, removing all the waters that overlapped with the proteins atoms (Fig. 5). To equilibrate the system, a series of stochastic boundary molecular dynamics (SBMD) were performed. First, the solute and the water molecules in the 16-Å sphere around the active site were subjected to a 10-ps SBMD simulation with a 12-Å reaction region and 1-fs timestep using SHAKE to constraint covalent bonds involving hydrogen. Afterwards, the SBMD simulation was carried out for 115 ps (15 ps of heating and equilibration, followed by 100 ps of production) with all atoms free to move. Non-bonded interactions were treated using a spherical cutoff of 13 Å with an atom-based potential shift method for van der Waals terms and the force-shift method for electrostatic terms. The system was minimized using the steepest descents (SD) and adaptive basis Newton-Raphson (ABNR) minimization algorithms. The resulting structure was used as the starting geometry for QM/MM calculations. During the dynamics His12 was not aligned properly to protonate the departing O₂ atom, but it was

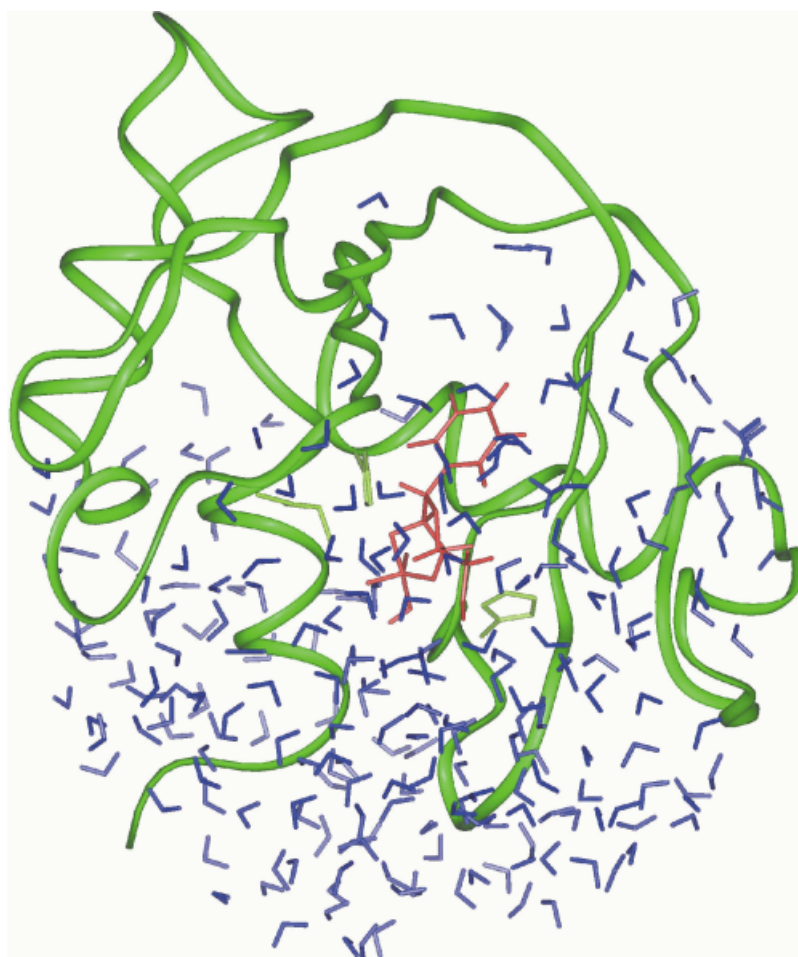


FIGURE 5. Uridine 2',3'-cyclic phosphorane-RNase A structure with a 16-Å water sphere around the phosphorus atom.

strongly hydrogen bonded to one of the phosphoryl oxygens O_{1P} (Fig. 6). The residue closest to $O_{2'}$ was Lys41. His119 maintained a hydrogen bond with O_{3P} for the duration of the simulation. This results are similar to inferences based on the crystal structure [47, 50].

Adiabatic Mapping of the Potential Energy Surface

The last structure of the dynamics described previously was used as the starting point for QM/MM calculations. The atoms defining the QM part are shown in Figure 6 and include the side chain of the His12 and His119, part of the side chain of Lys41, and part of uridine 2',3'-cyclic phosphorane (the pentacovalent phosphorane and the ribose ring). Hydrogen link atoms were introduced at the QM/MM boundary. A total of 55 QM atoms and

2535 MM atoms were present in the calculations, which included 231 water molecules. A 13-Å atom-based cutoff was considered for the MM-MM nonbonded interactions. The nonbonded interactions between the QM and MM parts were calculated without cutoff.

Initially, two series of resd minimizations were carried out (see above) departing from a dianionic phosphorane intermediate analog (Fig. 6) with restraints on the $P-O_{3P}$ and the $P-O_{2'}$ bonds, respectively. The $P-O_{3P}$ resd minimizations cover the part of the PES from the phosphorane intermediate passing to the reactants. During this first set of minimizations, we observed that elongation of the $P-O_{3P}$ bond was concerted with a proton transfer from the protonated His119 to O_{3P} to yield a water molecule (i.e., $O_{3P}H_2$). In the second case, resd minimizations with $P-O_{2'}$ as the restrained distance, the

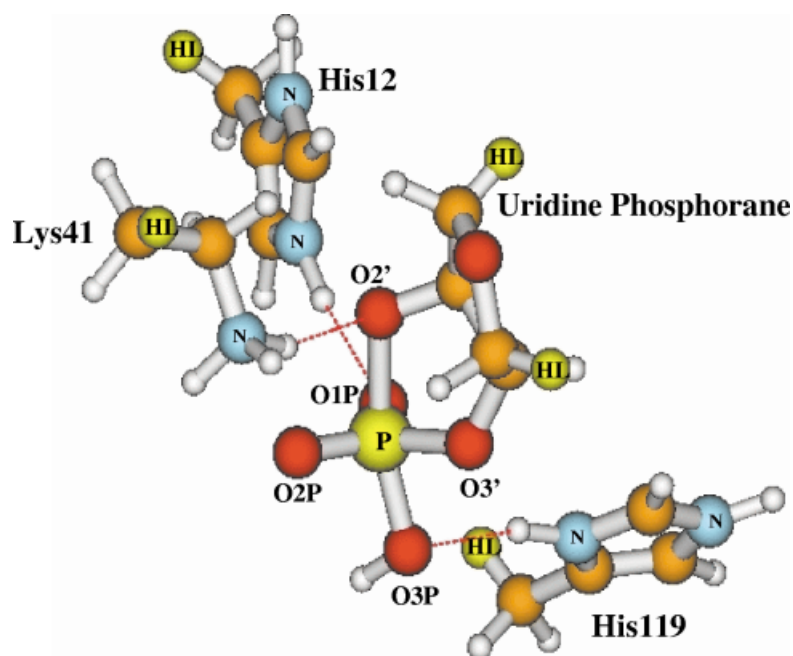


FIGURE 6. Definition of the quantum mechanical region in uridine 2',3'-cyclic phosphorane-RNase A. The sidechain of His12 and His119, part of the sidechain of Lys41, and the phosphorane and ribose subunits of the uridine 2',3'-cyclic phosphorane substrate were included in the QM region. HL indicates the hydrogen link atoms introduced in the system to treat the QM/MM boundary.

phosphorane intermediate passing to the phosphate monoester product. This step was also coupled with a proton transfer, in this case from Lys41 to $O_{2'}$.

To get a view of these two regions of the PES, we then carried restrained minimizations with two restrained distances. In Figure 7 the contour that correspond to these restrained minimizations are shown. The contour plot of Figure 7(A) corresponds to minimizations with restraints in the $P-O_{3P}$ distance (water attack on the phosphate) and the $N_{\delta}-H$ distance (i.e., proton transfer between His119 and O_{3P}); thus, this is the part of the potential energy surface that connects the reactant (uridine 2',3'-cyclic phosphate + water) to the intermediate uridine 2',3'-cyclic phosphorane. The reaction coordinate can be described mainly as a combination of these two variables. The water attack on the phosphate and the activation of the water by His119 occur in a step-wise fashion: the water approaches the reactant up to a distance of 1.9 Å, followed by a proton transfer from the water to His119. The rate-limiting step for the reaction is located in this region of the PES (see below).

Figure 7(B) shows a contour plot of the part of the PES that goes from the phosphorane intermediate

to the product. The two restraints are the the $P-O_{2'}$ distance and the $N_{\epsilon}-H$ distance (i.e., proton transfer between Lys41 and $O_{2'}$). There is a very shallow region in which the $P-O_{2'}$ bond is being opened with almost no barrier. As the $P-O_{2'}$ bond elongates accompanied by an increase in the negative charge localized on $O_{2'}$, which causes the protonated Lys41 to approach it, and provide the electrostatic stabilization of the negative charge. At a $P-O_{2'}$ distance of 2.4 Å, a proton is transferred from Lys41 to $O_{2'}$, and the energy of the system drops as the phosphate monoester product is formed.

We also carried out calculations in which the transfer of the proton to $O_{2'}$ was forced from His12 rather than from Lys41. The resultant product structure in which Lys41 is protonated and His12 is neutral (since it donated its proton to $O_{2'}$) is 9 kcal/mol higher in energy than the product with the Lys41 in its neutral state and His12 in its charged form. Neither protonation by Lys 41 nor by His 12 give rise to a detectable barrier [cf. Fig. 7(C)], so that it would be difficult to assess experimentally which protonation reaction actually occurs.

Additional QM/MM investigations of the proton transfer step are underway. The current calcu-

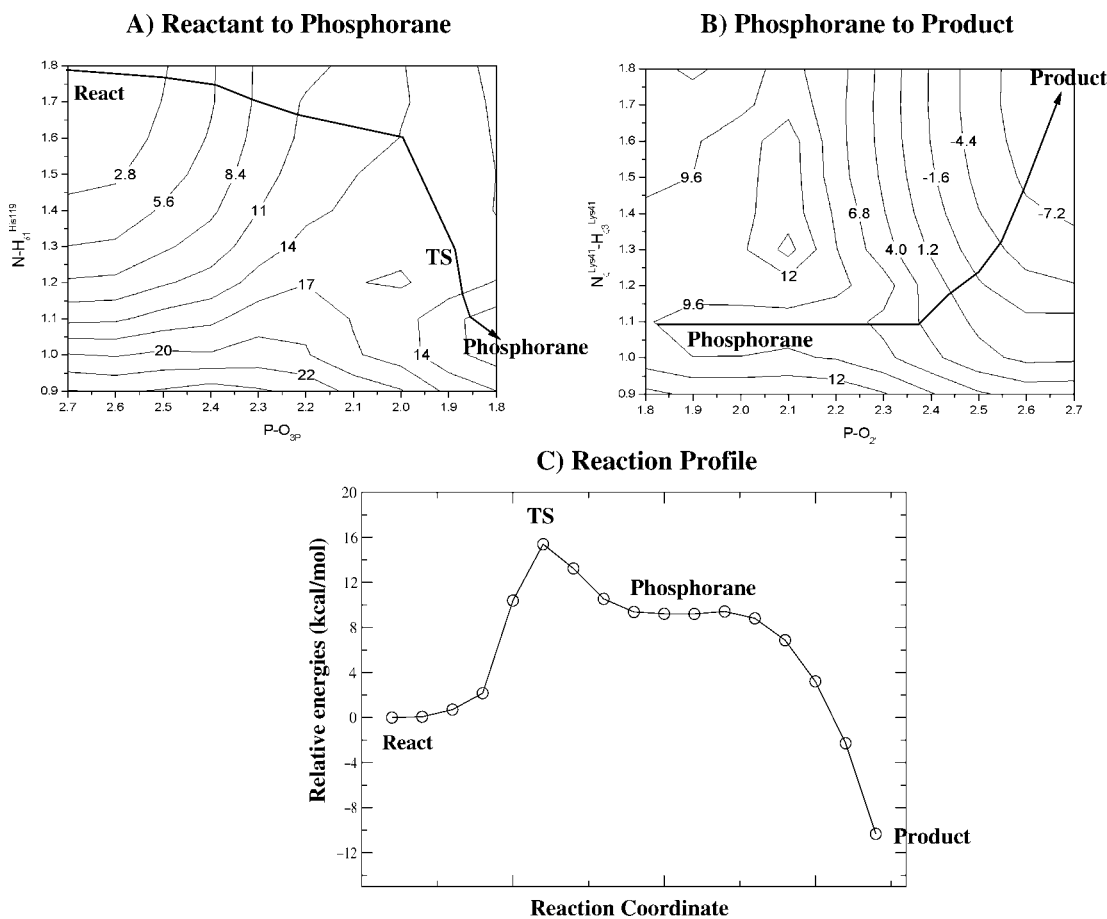


FIGURE 7. Contour plots of the PES for the hydrolysis of uridine 2',3'-cyclic phosphate in RNase A. Calculations were performed using the AM1/d-MM model: (A) contour plot corresponds to the part of the PES that goes from the reactant to the phosphorane intermediate and implies a nucleophilic attack of a water on the phosphate with proton transfer of the water to His119. (B) Contour plot of the PES going from the phosphorane intermediate to the phosphate monoester product by cleavage of the P-O_{2'} bond and proton transfer from Lys41. (C) Energy profile for the reaction. All numbers in the diagrams are relative energies in kcal/mol with respect to the reactant.

lations indeed do not include dynamic relaxation effects, which could be important for describing quantitatively the energetics of the proton transfer. Since Lys41 is more solvent exposed than His12, the positively charged Lys 41 should be favored by solvation, and solvation would therefore disfavor proton transfer from Lys 41. This effect may not be quantitatively accounted for by the QM/MM adiabatic mapping that we performed. Nevertheless, the present QM/MM energy minimizations suggest that Lys41 could be the residue involved in the proton transfer and acid activation of the O_{2'} atom rather than His12, as proposed in the standard mechanism. Wladkowski et al. have also suggested a more prominent role for Lys41, based on X-ray structures and ab initio quantum me-

chanical calculations of a detailed RNase A active site model [9, 10, 47]. However, they focus on the transphosphorylation step of the reaction rather than the hydrolysis step considered here.

Reaction Energies

Figure 7(C) shows the QM/MM energy profile for the hydrolysis reaction in RNase A. The geometries used in the profile were taken from the steepest descent path from the transition state toward the reactant and the phosphorane intermediate. From the phosphorane intermediate to the products, we selected geometries from the contour plot of Figure 7(B). The reaction can be divided in three different parts. First the water approaches the phosphate, with subsequent proton transfer from

the water to His119 (e.g., His119 is a base catalyst). The rate-determining transition state of the reaction is located in this part of the PES. Lys41 is stabilizing the excess of negative charge of the phosphorane by electrostatic interactions/hydrogen bonding with one of the equatorial oxygens (O_{2P}) and with the axial $O_{2'}$ oxygen. Our results are in agreement with the experimental finding [46] that the pK_a of the Lys41 group does not significantly affect the relaxation of the rate-limiting transition state of the reaction. However, our results differ somewhat from the conclusions drawn by Messmore et al. [46]. We do not see an enhancement of the hydrogen bond of Lys41 with one of the equatorial oxygens of the phosphorane, rather an electrostatic/hydrogen bond stabilization of O_{2P} and $O_{2'}$ appears to be involved.

Then the reaction goes through the phosphorane pentacovalent structures, which are on a shallow region of the PES. As the $P-O_{2'}$ bond is broken, electronic charge is transferred to $O_{2'}$, and Lys41

TABLE III
Relative energies (kcal/mol) of the transition state and product with respect to the reactant for the enzymatic reaction.^a

Reactant	AM1/d-MM	HF/6-31G(d)-MM	Exp.
TS	15.4	17.0	19.0
PROD	-10.3	-9.0	-4.0

^a Calculations done at the AM1/d-MM level of theory. HF/6-31G(d)-MM single-point energies at the AM1/d-MM geometries are also shown. The experimental estimates [15] for the reaction barrier and exothermicity of the reaction are also listed.

approaches $O_{2'}$. Finally, there is a proton transfer from Lys41 to $O_{2'}$ that leads to cleavage of the $P-O_{2'}$ bond and the formation of products. This step of the reaction does not have a significant barrier, and therefore, is expected to have a negligible effect

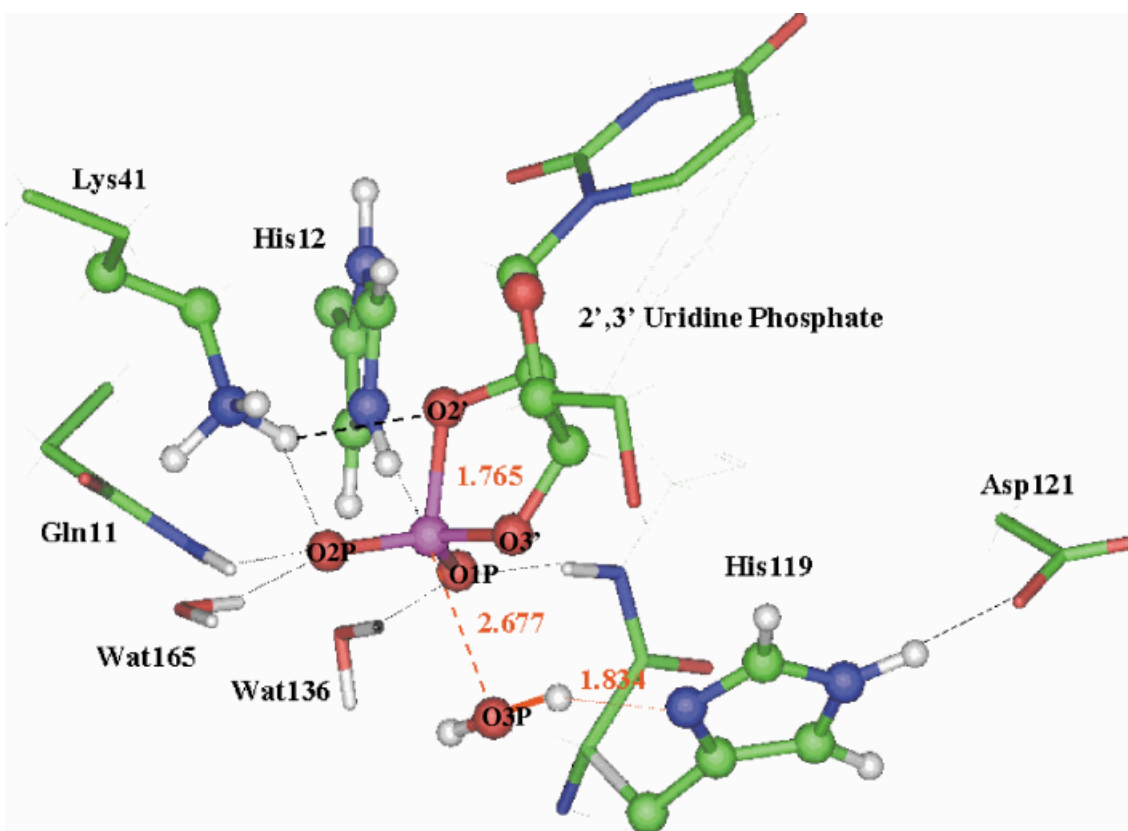


FIGURE 8. AM1/d-MM geometry of the uridine 2',3'-cyclic phosphate reactant bound to RNase A. Atoms considered in the QM part are depicted in ball-and-stick format. For sake of clarity, not all quantum hydrogens are shown. Selected hydrogen bonds are indicated with dashed lines. For values of relevant atomic distances see Table IV, column labeled react.

on the observed rate of the reaction. Consequently, most experiments would not be able to supply information on this step.

Table III lists the calculated and experimental values for the barrier and exothermicity of the reaction. The reaction barrier obtained at AM1/d-MM level of theory is 15.5 kcal/mol and the exothermicity of the reaction is -9.5 kcal/mol. Based on kinetic experiments [15], a barrier height of 19 kcal/mol and an exothermicity of -4 kcal/mol have been estimated. Our results are in reasonable agreement with these numbers. We also carried out single-point HF/6-31G(d)-MM calculations at the AM1/d-MM geometries for the reactant transition state and product of the reaction. The results for the barrier heights and the exothermicity of the reaction do not vary significantly, 17.0 and -9.0 kcal/mol, respectively. Notice that the barrier for the reaction is significantly lower than any of the barriers calculated for hydrolysis of ethylene phosphate in the

gas phase or in solution (see Tables I and II). Further insight into the enzyme mechanism is provided by the reactant, transition state, and product structures, as discussed below.

Structures

Structures for the reactant, transition state, and product of the reaction are depicted in Figures 8, 9, and 10, respectively. Values for selected distances in the three structures are listed in Table IV. The reactant structure corresponds to an uridine 2',3'-cyclic phosphate molecule with the attacking water 2.677 Å from the phosphorus atom. This water molecule is hydrogen bonded to the unprotonated His119 with a hydrogen bond distance of 1.859 Å. The negative charge of the uridine 2',3'-cyclic phosphate is concentrated on the phosphoryl oxygens O_{1P} and O_{2P}, and is stabilized by hydrogen bonds with residues of RNase A and two water molecules in the active site. The O_{1P} makes hydrogen bonds

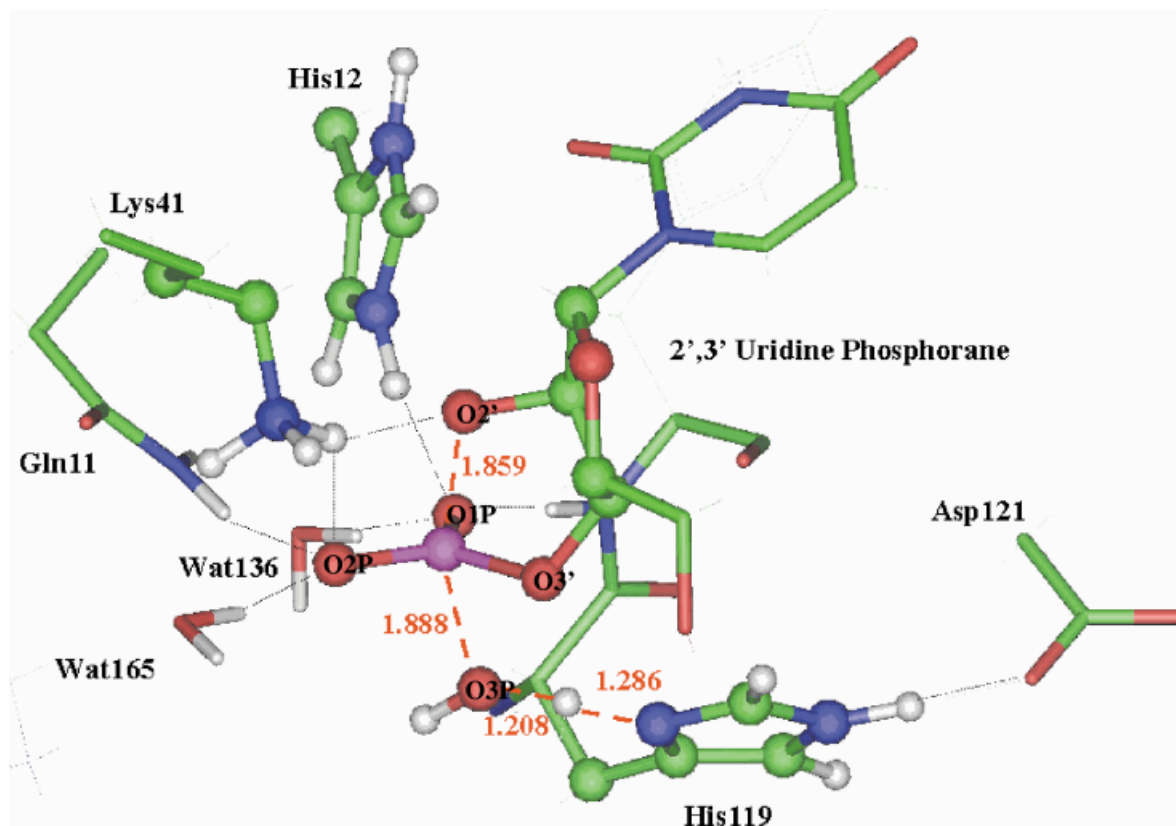


FIGURE 9. AM1/d-MM geometry of the transition state for the hydrolysis of RNA, catalyzed by RNase A. Atoms considered inside the QM part are depicted in ball-and-stick format. For sake of clarity, not all quantum hydrogens are shown. Selected hydrogen bonds are indicated with dashed lines. For values of relevant atomic distances see Table IV, column labeled TS.

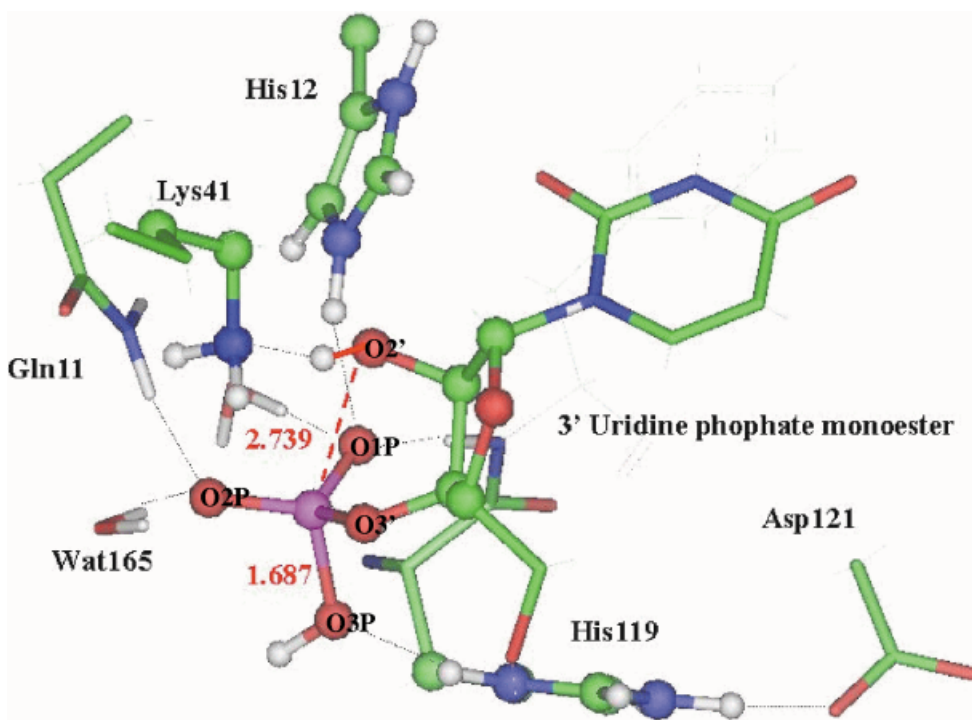


FIGURE 10. AM1/d-MM geometry of the uridine 3'-phosphate for the hydrolysis of RNA, catalyzed by RNase A. Atoms considered inside the QM part are depicted in ball-and-stick format. For sake of clarity, not all quantum hydrogens are shown. Selected hydrogen bonds are indicated with dashed lines. For values of relevant atomic distances see Table IV, column labeled Prod.

with H^{Phe120} of the backbone of Phe120 ($H^{\text{Phe120}}-O_{1P}$ distance is 1.994 Å), the side chain of His12 ($H_{\epsilon_2}^{\text{His12}}-O_{1P}$ distance is 2.060 Å), and one water molecule ($H_{\text{Wat136}}-O_{1P}$ distance is 1.817 Å). The O_{2P} phosphoryl oxygen makes hydrogen bonds with Lys41 ($H_{\zeta_3}^{\text{Lys41}}-O_{2P}$ distance is 1.803 Å), Gln11 ($H_{\epsilon_{21}}^{\text{Gln11}}-O_{2P}$ distance is 1.944 Å), and a water molecule ($H_{\text{Wat165}}-O_{2P}$ distance is 1.775 Å). The four P-O bond distances in the phosphate show the expected trend with the two phosphoryl oxygens having the shortest P-O bond lengths (1.531 and 1.539 Å for P- O_{1P} and P- O_{2P} , respectively) and the two phosphoester bonds having the largest bond lengths (1.761 and 1.700 Å for P- $O_{2'}$ and P- $O_{3'}$, respectively).

The transition state (Fig. 9) corresponds to the water attack with proton transfer from the attacking water to His119. The transition state shows a rather associative phosphorane structure with P- O_{3P} and P- $O_{2'}$ distances of 1.888 and 1.859 Å, respectively. The transferred proton ($H_{\delta_1}^{\text{His119}}$) is equally shared by O_{3P} and $N_{\delta_1}^{\text{His119}}$, with the $H_{\delta_1}^{\text{His119}}-O_{3P}$ distance of 1.208 Å and the $H_{\delta_1}^{\text{His119}}-N_{\delta_1}^{\text{His119}}$ distance of 1.286 Å. The P-OH distance and the degree of proton transfer show similarities to the structure of the gas-

phase neutral transition state $TS1^0$ (Fig. 3), even though the formal charge of the phosphorane is very different. However, the P- $O_{2'}$ bond is significantly longer than in $TS1^0$ (1.859 vs. 1.678 Å) and is in fact similar to the P- $O_{2'}$ bond found in the gas-phase dianionic $TS1^{-2}$ (1.860 Å). Thus, the enzyme has stabilized that part of the PES that corresponds to the nucleophilic attack, while it has maintained a good degree of P- $O_{2'}$ activation. The particular conformation of the residues around the phosphate/phosphorane substrate makes this possible. As the water attack takes place, the two phosphoryl oxygens O_{1P} and O_{2P} , and the phosphoester $O_{2'}$ oxygen accumulate charge. The excess negative charge on the two phosphoryl oxygens is stabilized through and enhancement of the hydrogen-bonded interactions with His12, the backbone amino group of Phe120 and Wat136 for O_{1P} , and Gln11 and Wat165 for O_{2P} . This is evidenced by a remarkable reduction in these hydrogen-bonded distance when we pass from the reactants to transition state (see Table IV). For instance, $H_{\epsilon_2}^{\text{His12}}-O_{1P}$ bond shows a reduction of 0.2 Å, i.e., from 2.060 Å in the reactant to 1.837 Å in the transition state. The only residue

TABLE IV
Selected atomic distances (in Å) for the reactant, transition state, and product structure of the hydrolysis of RNA catalyzed by RNase A.^a

	Reactant ^b	TS ^c	Prod ^b
H _{ε2} ^{His12} -O _{1P}	2.060	1.837	1.944
H ^{Phe120} -O _{1P}	1.994	1.844	1.875
H ^{Wat136} -O _{1P}	1.817	1.758	1.787
H _{ζ3} ^{Lys41} -O _{2P}	1.803	2.009	2.985
H _{ε21} ^{Gln11} -O _{2P}	1.944	1.862	1.775
H ^{Wat165} -O _{2P}	1.775	1.716	1.723
H _{ε2} ^{His12} -O _{2'}	2.563	2.438	2.227
H _{ζ3} ^{Lys41} -O _{2'}	2.828	2.145	1.024
N _ζ ^{Lys41} -H _{ζ3} ^{Lys41}	1.065	1.069	1.786
O _{3P} -H _{δ1} ^{His119}	1.004	1.208	1.911
N _{δ1} ^{His119} -H _{δ1} ^{His119}	1.859	1.286	1.044
P-O _{3P}	2.744	1.888	1.688
P-O _{2'}	1.761	1.859	2.703
P-O _{3'}	1.700	1.743	1.707
P-O _{1P}	1.531	1.560	1.548
P-O _{2P}	1.539	1.554	1.537

^a All structures were obtained using the AM1/d-MM level of theory using CHARMM.

^b Optimized using the adaptive basis Newton-Raphson (ABNR) method.

^c Optimized using the conjugate peak refinement (CPR) algorithm.

that does not show this behavior is Lys41. Instead of enhancing its interaction with O_{2P}, the H_{ζ3}^{Lys41}-O_{2P} distance increases from 1.803 Å in the reactant to 2.009 Å in the transition state, as the positively charged Lys41 residue migrates toward the O_{2'} axial atom. Thus, the H_{ζ3}^{Lys41}-O_{2'} distance decreases from 2.828 Å in the reactant to 2.145 Å in the transition state. The flexibility of the long side chain of Lys41 plays a very important role, which allows Lys41 to interact primarily with O_{2P} in the reactant, then with O_{2P} and O_{2'} in the transition state, and to finally protonate this atom. At the TS, there is no degree of proton transfer from Lys41. In this sense, the present mechanism gives support to Messmore's [46] observation that the pK_a of residue 41 does not have a

large effect on the rate-limiting transition state of the reaction.

The phosphate monoester product structure is shown in Figure 10. The P-O_{2'} distance is 2.739 Å and the P-O_{3P} bond length is 1.687 Å. The now neutral Lys41 is hydrogen bonded to the proton of O_{2'}. The three hydrogen bonds to O_{1P} have lengthened with respect to those of the transition state. However, the two hydrogen bond interactions with O_{2P} are either enhanced (H_{ε21}^{Gln11}-O_{2P} distance is 1.775 Å) or only slightly modified (H^{Wat165}-O_{2P} is 1.723 Å) with respect to the transition state, as they need to compensate for the loss of the Lys41-O_{2P} hydrogen bond interaction. The protonated His119 maintains a hydrogen bond with O_{3P}.

How Does RNase A Work?

We have shown that the rate-limiting TS for the hydrolysis of uridine 2',3'-cyclic phosphate in RNase A corresponds to the approach of a water molecule to the phosphate and its activation by His119. Thus, His119 is a generalized base catalyst, removing the proton from the approaching water molecule. This leads to a significant increase in the negative charge density of the phosphorane. Effective stabilization of this negative charge density is important for the rate enhancement. This is accomplished through a combination of electrostatic and hydrogen bonded interactions. The protonated His12 stabilizes the accumulation of negative charge density on O_{1P} through a hydrogen bond interaction. Lys41 stabilizes the negative charge of O_{2P} and O_{2'}. Other residues such as Phe120 and Gln11 also have a direct interaction with the substrate, although experimental evidence [52] indicates that they are less important for catalysis.

After the rate-limiting transition state, we enter a very shallow part of the potential energy surface. Here there is a very unstable pentacovalent phosphorane, and the P-O_{2'} bond can be broken with no detectable barrier. The positively charged Lys41 first stabilizes the accumulation of negative charge density at O_{2'} and finally protonates this atom, although dynamic effects could alter this behavior.

Conclusion

In this study, we have presented theoretical results for the hydrolysis of phosphate diesters in a variety of environments: gas phase, solution, and

enzyme. These calculations demonstrate how combined density functional, semiempirical and molecular mechanical models can be used in concert to provide a comprehensive picture of a fundamental and challenging biological reaction: phosphate hydrolysis catalyzed by RNase A. From the gas-phase calculations, we observed that the neutralization of negative charge in the phosphorane greatly increased the stability of the structures and was a key factor to accelerate the hydrolysis. Solvent effectively stabilizes the negative charge in the case of the alkaline hydrolysis of phosphate diesters. Moreover, we have determined that solvent is intimately related to the observed trends in reactivity for phosphates. The fact that cyclic phosphates are hydrolyzed much faster than their acyclic counterparts is mainly a solvent effect rather than a consequence of the ring strain in cyclic compounds. Finally, we have analyzed the catalytic mechanism of bovine ribonuclease A. A variety of specific enzyme-substrate interactions act together: acid/base catalysis, hydrogen bonding, and electrostatic stabilization. Hybrid QM/MM methods are essential tools to model quantum mechanical effects in complex chemical environments, and provide key insight in the catalytic mechanisms of enzymes.

ACKNOWLEDGMENT

X.L. is funded by the European Commission through a Marie-Curie Research training grant. D.Y. is grateful for financial support provided by the National Institutes of Health, the Minnesota Supercomputing Institute, and the Donors of The Petroleum Research Fund, administered by the American Chemical Society. We thank the Institut de Développement et des Ressources en Informatique Scientifique (IDRIS) for a generous allocation of CRAY computer time. We also thank Prof. W. Thiel for very useful discussions on the MNDO97 program.

References

- Voet, D.; Voet, J. G.; Pratt, C. W. *Fundamentals of Biochemistry*; Wiley: New-York, 1998.
- Oivanen, M.; Kuusela, S.; Lonnberg, H. *Chem Rev* 1998, 98, 1102-1109.
- Perreault, D. M.; Anslyn, E. V. *Angew Chem Int Ed Engl* 1997, 36, 432-450.
- Uchamaru, T.; Tanabe, K.; Nishikawa, S.; Taira, K. *J Am Chem Soc* 1991, 113, 4351-4353.
- Dejaegere, A.; Lim, C.; Karplus, M. *J Am Chem Soc* 1991, 113, 4353-4355.
- Lim, C.; Tole, P. *J Phys Chem* 1992, 96, 5217-5219.
- Dejaegere, A.; Liang, X.; Karplus, M. *J Chem Soc Faraday Trans* 1994, 90, 1763-1770.
- Colvin, M. E.; Evleth, E.; Akacem, Y. *J Am Chem Soc* 1995, 117, 4357-4362.
- Wladkowski, B. D.; Krauss, M.; Stevens, W. J. *J Phys Chem* 1995, 99, 6273-6276.
- Wladkowski, B. D.; Krauss, M.; Stevens, W. J. *J Am Chem Soc* 1995, 117, 10537-10545.
- Florián, J.; Warshel, A. *J Phys Chem B* 1998, 102, 719-734.
- Mercero, J. M.; Barrett, P.; Lam, C. W.; Fowler, J. E.; Ugalde, J. M.; Pedersen, L. G. *J Comput Chem* 2000, 21, 43-51.
- Richards, F.; Wyckoff, H. *Enzymes* 1971, IV, 647-806.
- Blackburn, P.; Moore, S. *Pancreatic Ribonuclease. The Enzymes*; Academic: New York, 1982.
- Raines, R. *Chem Rev* 1998, 98, 1045-1065.
- Fersht, A. *Structure and Mechanism in Protein Science*; W. H. Freeman: New York, 1999.
- Haydock, K.; Lim, C.; Brunger, A.; Karplus, M. *J Am Chem Soc* 1990, 112, 3826-3831.
- Lopez, X.; Dejaegere, A.; Karplus, M. *J Am Chem Soc* 1999, 121, 5548-5558.
- Tomasi, J.; Persico, M. *Chem Rev* 1994, 94, 2027-2094.
- Cossi, M.; Barone, V.; Cammi, R.; Tomasi, J. *Chem Phys Lett* 1996, 255, 327-335.
- Mineva, T.; Russo, N.; Sicilia, E. *J Comput Chem* 1998, 19, 290-299.
- Bash, P. A.; Field, M. J.; Karplus, M. *J Am Chem Soc* 1987, 109, 8092-8094.
- Field, M. J.; Bash, P. A.; Karplus, M. *J Comp Chem* 1990, 11, 700-733.
- Bash, P. A.; Ho, L. L.; MacKerell, J.; Levine, D.; Hallstrom, P. *Proc Nat Acad Sci* 1996, 93, 3698-3703.
- Becke, A. *Phys Rev A* 1988, 38, 3098-3100.
- Lee, C.; Yang, W.; Parr, R. G. *Phys Rev B* 1988, 37, 785.
- Vosko, S. H.; Wilk, L.; Nusair, M. *Can J Phys* 1980, 58, 1200.
- Becke, A. *J Chem Phys* 1993, 98, 1372-1377.
- Curtiss, L. A.; Raghavachari, K.; Trucks, G. W.; Pople, J. A. *J Chem Phys* 1991, 94, 7221-7230.
- Frisch, M. J.; Trucks, G. W.; Schlegel, H. B.; Scuseria, G. E.; Robb, M. A.; Cheeseman, J. R.; Zakrzewski, V. G.; Montgomery, J. A.; Stratmann, R. E.; Burant, J. C.; Dapprich, S.; Millam, J. M.; Daniels, A. D.; Kudin, K. N.; Strain, M. C.; Farkas, J. T.; Barone, V.; Cossi, M.; Cammi, R.; Mennucci, B.; Pomelli, C.; Adamo, C.; Clifford, S.; Ochterski, J.; Petersson, G. A.; Ayala, P. Y.; Cui, Q.; Morokuma, K.; Malick, D. K.; Rabuck, A. D.; Raghavachari, K.; Foresman, J. B.; Cioslowski, J.; Ortiz, J. V.; Stefanov, B. B.; Liu, G.; Liashenko, A.; Piskorz, P.; Komaromi, I.; Gomperts, R.; Martin, R. L.; Fox, D. J.; Keith, T.; Al-Laham, M. A.; Peng, C. Y.; Nanayakkara, A.; Gonzalez, C.; Challacombe, M.; Gill, P. M. W.; Johnson, B. G.; Chen, W.; Wong, M. W.; Andres, J. L.; Head-Gordon, M.; Replogle, E. S.; Pople, J. A. *Gaussian 98 (Revision A.2)*; Gaussian: Pittsburgh, 1998.
- Frisch, M. J.; Trucks, G. W.; Schlegel, H. B.; Scuseria, G. E.; Robb, M. A.; Cheeseman, J. R.; Zakrzewski, V. G.; Montgomery, J. A.; Stratmann, R. E.; Burant, J. C.; Dapprich, S.; Millam, J. M.; Daniels, A. D.; Kudin, K. N.; Strain,

- M. C.; Farkas, J. T.; Barone, V.; Cossi, M.; Cammi, R.; Men-
nucci, B.; Pomelli, C.; Adamo, C.; Clifford, S.; Ochterski,
J.; Petersson, G. A.; Ayala, P. Y.; Cui, Q.; Morokuma, K.;
Malick, D. K.; Rabuck, A. D.; Raghavachari, K.; Foresman,
J. B.; Cioslowski, J.; Ortiz, J. V.; Stefanov, B. B.; Liu, G.;
Liashenko, A.; Piskorz, P.; Komaromi, I.; Gomperts, R.; Mar-
tin, R. L.; Fox, D. J.; Keith, T.; Al-Laham, M. A.; Peng,
C. Y.; Nanayakkara, A.; Gonzalez, C.; Challacombe, M.; Gill,
P. M. W.; Johnson, B. G.; Chen, W.; Wong, M. W.; Andres,
J. L.; Head-Gordon, M.; Replogle, E. S.; Pople, J. A. *Gaussian*
94; Gaussian: Pittsburgh, 1995.
32. Gao, J. *Rev Comput Chem* 1995, 7, 119–185.
 33. Lopez, X.; York, D. M.; Karplus, M., to appear.
 34. Thiel, W. Program MNDO97; University of Zurich: Zurich,
1998.
 35. MacKerell, Jr., A. D.; Bashford, D.; Bellott, M.; Dunbrack, Jr.,
R. L.; Evanseck, J. D.; Field, M. J.; Fischer, S.; Gao, J.; Guo, H.;
Ha, S.; Joseph-McCarthy, D.; Kuchnir, L.; Kuczera, K.; Lau,
F. T. K.; Mattos, C.; Michnick, S.; Ngo, T.; Nguyen, D. T.;
Prodhom, B.; Reiher III, W. E.; Roux, B.; Schlenkrich, M.;
Smith, J. C.; Stote, R.; Straub, J.; Watanabe, M.; Wiórkiewicz-
Kuczera, J.; Yin, D.; Karplus, M. *J Phys Chem B* 1998, 102,
3586–3616.
 36. Brooks, B. R.; Brucoleri, R. E.; Olafson, B. D.; States, D. J.;
Karplus, M. *J Comput Chem* 1983, 4, 187–217.
 37. Fischer, S.; Karplus, M. *Chem Phys Lett* 1992, 194, 252–261.
 38. Westheimer, F. *Acc Chem Res* 1968, 1, 70–78.
 39. Westheimer, F. *Science* 1987, 235, 1173–1178.
 40. Findlay, D.; Herries, D.; Mathias, A.; Rabin, B.; Ross, C.
Nature 1961, 190, 781–784.
 41. Anslyn, E.; Breslow, R. *J Am Chem Soc* 1990, 112, 9621–9623.
 42. Breslow, R.; Huang, D.-L. *J Am Chem Soc* 1990, 112, 9621–
9623.
 43. Breslow, R.; Dong, S. D.; Xu, R. *J Am Chem Soc* 1996, 118,
6588–6600.
 44. Lim, C.; Tole, P. *J Am Chem Soc* 1992, 114, 7245–7254.
 45. Tole, P.; Lim, C. *J Phys Chem* 1993, 97, 6212–6219.
 46. Messmore, J. M.; Fuchs, D. N.; Raines, R. T. *J Am Chem Soc*
1995, 117, 8057–8060.
 47. Wladkowski, B. D.; Svensson, L. A.; Sjolín, L.; Ladner, J. E.;
Gilliland, G. L. *J Am Chem Soc* 1998, 120, 5488–5498.
 48. Glennon, T. M.; Warshel, A. *J Am Chem Soc* 1998, 120,
10234–10247.
 49. Warshel, A. *Computer Modeling of Chemical Reactions in*
Enzymes and Solutions; Wiley: New York, 1991.
 50. Ladner, J.; Wladkowski, B.; Svensson, L.; Sjolín, L.; Gilliland,
G. *Acta Crystallogr D* 1997, D53, 290–301.
 51. Brunger, A.; Karplus, M. *Proteins* 1988, 4, 148.
 52. delCardayre, S.; Ribo, M.; Yokel, E.; Quirk, D.; Rutter, W.;
Raines, R. *Protein Eng* 1995, 8, 261–273.